Brain Structure and Function (2021) 226:1909–1923
https://doi.org/10.1007/s00429-021-02300-0

ORIGINAL ARTICLE

The nucleus accumbens and ventral pallidum exhibit greater dopaminergic innervation in humans compared to other primates

Kristen N. Hirter[1,2] · Elaine N. Miller[3] · Cheryl D. Stimpson[3] · Kimberley A. Phillips[4,5] · William D. Hopkins[6] · Patrick R. Hof[7] · Chet C. Sherwood[3] · C. Owen Lovejoy[1,2] · Mary Ann Raghanti[1,2]

Received: 22 October 2020 / Accepted: 10 May 2021 / Published online: 25 May 2021

Abstract

Recent evidence suggests that increased dopaminergic signaling within the dorsal striatum played a central role in the evolution of the human brain. This increase has been linked to human prosociality and language in what has been described as a dopamine-dominated striatum personality style. Increased striatal dopamine is associated with an increase in ventral striatal activity and promotes externally driven behaviors, including cooperation and social conformity. In contrast, decreased striatal dopamine is associated with increased dorsal striatal activity and favors internally driven and goal-oriented behaviors. Previous comparative studies have focused on the dorsal striatum, measuring dopaminergic innervation in the dorsal and medial caudate nucleus and putamen. Here, we add to this knowledge by examining regions of the ventral striatum. We quantified the density of tyrosine hydroxylase–immunoreactive axons, as a measure of dopaminergic innervation, in the nucleus accumbens and ventral pallidum of humans, great apes, platyrrhine and cercopithecid monkeys. Our data show that humans have a significantly greater dopaminergic innervation in both structures, supporting the hypothesis that selection for a prosocial neurochemistry in the human basal ganglia may have contributed to the evolution of our uniquely social behavior profile.

Keywords Nucleus accumbens · Ventral pallidum · Tyrosine hydroxylase · Human evolution

Introduction

The striatum is a component of the nigrostriatal and mesolimbic dopaminergic pathways that facilitate motor production and reward regulation, respectively (Arias-Carrión et al. 2010; Haber 2003). The nigrostriatal pathway connects the substantia nigra pars compacta with the dorsal striatum (caudate nucleus and putamen), while the mesolimbic pathway connects the ventral tegmental area (VTA) to the ventral striatum, mediating pleasurable experiences (Báez-Mendoza et al. 2013; Haber 2003). The mesolimbic dopaminergic reward pathway is part of the brain's primary mechanism for encoding reward, and has been the subject of numerous clinical studies, as it can be targeted by addictive drugs (Kalivas and Volkow 2005; Volkow and Morales 2015). From an evolutionary standpoint, the reward system can perpetuate behaviors that enhance fitness by linking successful ones to elevated dopamine (DA) (Haber 2003; O'Connell and Hofmann 2011).

The striatum thus plays a major role in modulating social behaviors, particularly those involved in reward. It is, therefore, of interest that dorsal and ventral regions are

✉ Kristen N. Hirter
khirter@kent.edu

✉ Mary Ann Raghanti
mraghant@kent.edu

1 Department of Anthropology and School of Biomedical Sciences, Kent State University, Kent, OH, USA

2 Brain Health Research Institute, Kent State University, Kent, OH, USA

3 Department of Anthropology and Center for the Advanced Study of Human Paleobiology, The George Washington University, Washington, DC, USA

4 Department of Psychology, Trinity University, San Antonio, TX, USA

5 Southwest National Primate Research Center, Texas Biomedical Research Institute, San Antonio, TX, USA

6 Department of Comparative Medicine, University of Texas MD Anderson Cancer Center, Bastrop, TX, USA

7 Nash Family Department of Neuroscience and Friedman Brain Institute, Icahn School of Medicine at Mount Sinai, New York, NY, USA

functionally distinct (Báez-Mendoza et al. 2013; Báez-Mendoza and Schultz 2013; van den Bos 2015). The dorsal region is involved in internally motivated, goal-directed behavior, whereas the ventral region regulates behaviors that are externally guided and is associated with various limbic structures of the brain (van den Bos 2015). Moreover, the ventral striatum is thought to facilitate behavioral flexibility by promoting greater sensitivity to social and environmental cues, thus contributing to cooperation and social conformity in humans (Klucharev et al. 2009; Stallen and Sanfey 2015; van den Bercken and Cools 1982; Zaki et al. 2011). Neurotransmitter concentrations largely regulate differential activity in the striatum with high levels of acetylcholine favoring activity in the dorsal region and its associated internally motivated behaviors, and increased DA promoting externally guided behaviors that are regulated by the ventral region (Cools et al. 1990; Cools et al. 1975; van den Bercken and Cools 1982; van den Bos 2015). These results suggest that individual striatal neurochemical profiles predict individual-specific behaviors and personality style. Inter-individual differences in this system may provide a target for selection by favoring particular behaviors in different environments, and may, therefore, underlie species-specific social and behavioral adaptations.

Recently, Raghanti et al. (2016, 2018) reported that humans, compared to other primates, exhibit a unique striatal neurochemical signature that includes greater DA, serotonin, and neuropeptide Y but decreased acetylcholine in specific regions of the dorsal striatum. The present study builds on these earlier findings by directly quantifying DAergic innervation in the ventral striatum (i.e., nucleus accumbens, NAcc) and ventral pallidum (VP) with the goal of determining if greater DAergic transmission also extends to these regions as well. The NAcc is the ventromedial portion of the ventral striatum with afferent connections with the amygdala and regions of the prefrontal cortex (Haber and McFarland 1999; Haber et al. 1995, 2006). The VP, located ventral and adjacent to the anterior commissure, receives GABAergic projections from the ventral striatum and projects to additional brain regions that regulate motivation (e.g., Haber and Knutson 2010). The NAcc and VP are part of the reward system, with the NAcc playing a role in motivational and emotional responses to environmental stimuli and the VP involved in encoding the value of reward as well as the motor actions required to attain reward (e.g., Haber and McFarland 1999; Tachibana and Hikosaka 2012). Elevated DA in the NAcc has been linked to social conformity, compassion, and altruism (Filkowski et al. 2016; Klimecki et al. 2014; Klucharev et al. 2009; Stallen and Sanfey 2015). Higher levels of DA in the ventral striatum have also been linked to monogamy in some rodents (Aragona et al. 2006) and increased glucose uptake in both the NAcc and VP has been reported for pair-bonded versus lone male titi monkeys (Bales et al. 2007). Monogamy in these species includes biparental care, aggression towards unfamiliar conspecifics, and pair bonding (i.e., partner preference, but not sexual fidelity) (e.g., Young et al. 1998; Young and Wang 2004).

Humans are among the few species that are characterized by social monogamy, a behavioral complex hypothesized to consist of elevated intragroup cooperation, habitual upright walking, and virtual elimination of the canine crown's capacity to either serve as a weapon or signal of aggressive intent (Lovejoy 1981, 2009, 2014). We anticipated that monogamous, or semi-monogamous, species within our sample (humans, tamarins, marmosets, and owl monkeys) would possess significantly higher DA within the VP compared to non-monogamous species. We further anticipated that humans would possess higher DA within the NAcc which could account for our uniquely high levels of social conformity and capacity for compassion and altruistic acts.

Materials and methods

Specimens

We processed postmortem brain samples from 50 individuals across nine primate genera. Subjects included platyrrhines (cotton-top tamarins, common marmosets, owl monkeys, and tufted capuchins), cercopithecids (pig-tailed and rhesus macaques), African great apes (chimpanzees and bonobos), and humans (see Table 1 for details). Sexes were balanced as much as possible. All individuals were adult, free of gross neuropathology. Nonhuman primates had been housed in accordance with their home institution's animal care and use standards. We obtained the human brain specimens from the Northwestern University Alzheimer's Disease Center Brain Bank and the NIH NeuroBioBank. All individuals were non-geriatric and free of neuropathological disease. We received whole brains or sections for nonhuman primates from the National Chimpanzee Brain Resource, The Great Ape Neuroscience Project, the Oregon National Primate Research Center, the Washington National Primate Research Center, the New England Regional Primate Research Center (Harvard University), Alpha Genesis, and various zoos. Brain samples were fixed by immersion in 10% buffered formalin for 7–10 days, then transferred to a solution of 0.1 M phosphate-buffered saline (PBS, pH 7.4) containing 0.1% sodium azide and stored at 4 °C until further processing.

Sample processing

All samples were cryoprotected in a graded series of sucrose solutions (10, 20, and 30%) prior to sectioning. The brain samples were rapidly frozen with dry ice and then sectioned at 40 µm using a freezing sliding microtome (SM2000R,

Table 1 Subjects included in analyses

Species	Common name	Sex	Age (years)	PMI	Sexual maturity	Longevity (years)
Callithrix jacchus	Common marmoset	M	4.5	–	11–24 months	22.8
Callithrix jacchus	Common marmoset	M	2.75	–	11–24 months	22.8
Callithrix jacchus	Common marmoset	M	6	–	11–24 months	22.8
Callithrix geoffroyi	Geoffroy's marmoset	M	5.7	–	11–24 months	17.6
Callithrix geoffroyi[b]	Geoffroy's marmoset	M	8.5	–	11–24 months	17.6
Callithrix pygmaeus	Pygmy marmoset	F	11.25	–	18–24 months	18.6
Saguinus oedipus	Cotton-top tamarin	M	10.9	–	18–24 months	26.2
Saguinus oedipus	Cotton-top tamarin	M	8.4	–	18–24 months	26.2
Saguinus oedipus	Cotton-top tamarin	M	9.5	–	18–24 months	26.2
Saguinus oedipus	Cotton-top tamarin	F	10	–	18–24 months	26.2
Saguinus oedipus	Cotton-top tamarin	F	10	–	18–24 months	26.2
Saguinus oedipus	Cotton-top tamarin	F	10	–	18–24 months	26.2
Aotus trivirgatus[a]	Northern owl monkey	M	>18	–	2 years	30.1
Aotus spp.	Owl monkey	M	18	–	2 years	27
Aotus spp.	Owl monkey	F	3	–	2 years	27
Aotus vociferans	Spix's night monkey	F	5	–	2 years	22.1
Cebus apella	Tufted capuchin	M	2.9	–	4–8 years	46
Cebus apella	Tufted capuchin	M	16.6	–	4–8 years	46
Cebus apella	Tufted capuchin	M	15.9	–	4–8 years	46
Cebus apella	Tufted capuchin	F	12.6	–	4–8 years	46
Cebus apella	Tufted capuchin	F	17.5	–	4–8 years	46
Cebus apella	Tufted capuchin	F	18.3	–	4–8 years	46
Macaca mulatta	Rhesus macaque	M	8	–	2.5–8 years	40
Macaca mulatta	Rhesus macaque	M	13	–	2.5–8 years	40
Macaca mulatta	Rhesus macaque	M	13	–	2.5–8 years	40
Macaca mulatta	Rhesus macaque	F	14	–	2.5–8 years	40
Macaca mulatta	Rhesus macaque	F	11	–	2.5–8 years	40
Macaca mulatta	Rhesus macaque	F	12.5	–	2.5–8 years	40
Macaca nemestrina	Pigtailed macaque	M	15.73	–	2.5–8 years	37.6
Macaca nemestrina	Pigtailed macaque	M	4.28	–	2.5–8 years	37.6
Macaca nemestrina	Pigtailed macaque	M	2.5	–	2.5–8 years	37.6
Macaca nemestrina	Pigtailed macaque	F	15.1	–	2.5–8 years	37.6
Macaca nemestrina	Pigtailed macaque	F	14	–	2.5–8 years	37.6
Macaca nemestrina	Pigtailed macaque	F	5.95	–	2.5–8 years	37.6
Pan troglodytes	Chimpanzee	M	19.8	–	7–9 years	59.4
Pan troglodytes	Chimpanzee	M	19.5	–	7–9 years	59.4
Pan troglodytes	Chimpanzee	F	30.8	–	7–9 years	59.4
Pan troglodytes	Chimpanzee	F	18.5	–	7–9 years	59.4
Pan troglodytes[a]	Chimpanzee	F	17.8	–	7–9 years	59.4
Pan paniscus	Bonobo	M	34	–	7–9 years	55
Pan paniscus	Bonobo	M	5	–	7–9 years	55
Pan paniscus	Bonobo	M	25	–	7–9 years	55
Pan paniscus	Bonobo	F	52	–	7–9 years	55
Pan paniscus[a]	Bonobo	F	25	–	7–9 years	55
Homo sapiens	Human	M	44	19		
Homo sapiens	Human	M	56	15		
Homo sapiens	Human	M	44	24		
Homo sapiens	Human	F	39	19		
Homo sapiens	Human	F	25	12		
Homo sapiens	Human	F	53	17		

Postmortem interval (PMI) is provided for humans. Specific PMI for nonhuman specimens was not available, but < 24 h. Average age for sexual maturity and lifespan are provided for nonhuman primates (Nowak 1999; AnAge Database, https://genomics.senescence.info/species/index.html)

[a]Only included in among-species analysis for NAcc

[b]Only included in among-species analysis for VP

Leica, Chicago, IL, USA). Each section was placed into an individual centrifuge tube containing freezer storage solution (30% each distilled water, ethylene glycol, and glycerol and 10% 0.244 M PBS), numbered sequentially, and then stored at – 20 °C until histological or immunohistochemical processing. Every tenth section was Nissl-stained to visualize the regions of interest for immunohistochemical staining and stereological quantification of neuron cell density.

Figures 1 and 2 show the two areas of interest for the present study: the NAcc, which comprises most of the ventral striatum and in this study we conservatively defined as the portion of the ventromedial striatum that is ventral and medial to the inferior border of the internal capsule in sections rostral to the appearance of the anterior commissure; the VP, which was traced in sections ventral and adjacent to the anterior commissure with readily discernable borders (Paxinos et al. 2000, 2012; Haber and McFarland 1999). We did not differentiate between the shell and core region of the NAcc in this study as TH does not provide clear boundaries between these regions (e.g., McCollum et al. 2016).

Immunohistochemistry

Sections that spanned the NAcc and VP for each subject were stained for tyrosine hydroxylase (TH), the rate-limiting enzyme for catecholamine synthesis, using the avidin–biotin–peroxidase method as described previously (Raghanti et al. 2008, 2009, 2016). Briefly, sections were pretreated for antigen retrieval by incubating in 0.05% citraconic acid (pH 7.4) at 86 °C in a water bath for 30 min. Sections were then rinsed, and endogenous peroxidase was quenched using a solution of 75% methanol, 2.5% hydrogen peroxide (30%), and 22.5% distilled water for 20 min at room temperature. Sections were pre-blocked in a solution of 4% normal goat serum, 0.6% Triton X-100 detergent, 90.4% PBS, and 5% bovine serum albumin. Following this, sections were incubated in a rabbit anti-TH polyclonal antibody (Millipore, Bedford, MA, AB152, RRID 390204) diluted to 1:1000 for 24 h at room temperature followed by 24 h at 4 °C. Sections were then incubated in a biotinylated secondary antibody (1:200) followed by the avidin–peroxidase complex (PK-6100, Vector Laboratories, Burlingame, CA) for 1 h at room temperature. A 3,3′-diaminobenzidine–peroxidase (DAB) substrate with nickel solution enhancement was used as the chromogen (SK-4100, Vector Laboratories).

Data acquisition

Quantitative analyses were performed using computer-assisted stereology on an Olympus BX-51 photomicroscope system equipped with a digital camera and StereoInvestigator software version 10 (MBF Bioscience, Williston, VT, USA). Subsampling techniques were performed for each species to determine appropriate sampling parameters. TH–immunoreactive (ir) axons were quantified using the SpaceBalls probe at 100x (N.A. 1.4) magnification under Koehler illumination using a hemisphere set at 7 µm with a 2% guard zone. Section thickness was measured at every fifth sampling site with an average mounted section thickness for immunostained sections being 23.9 ± 8.2 µm.

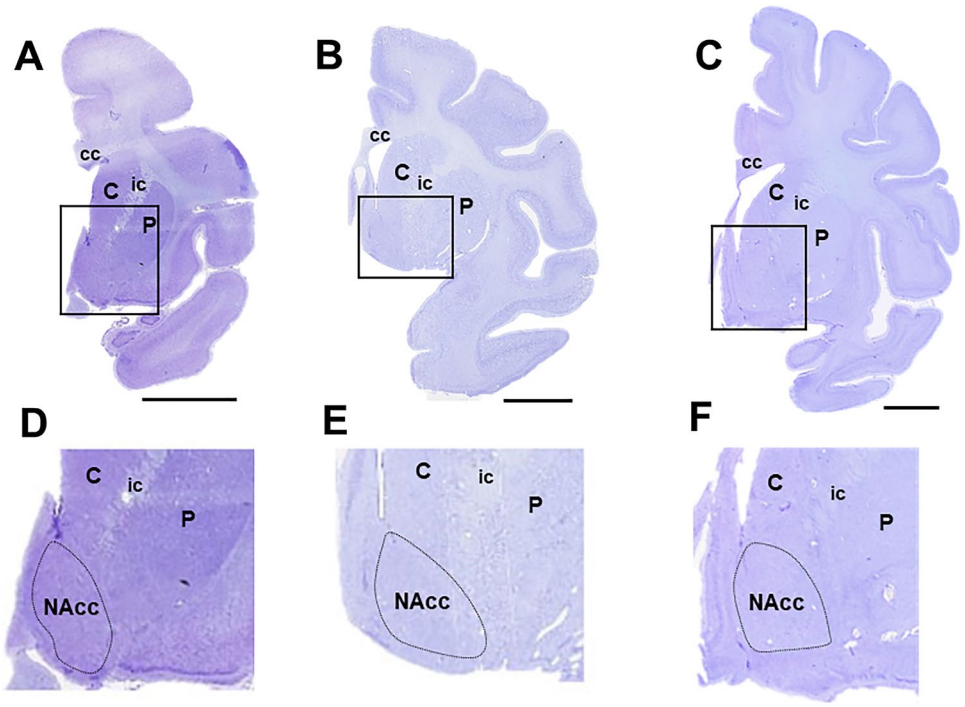

Fig. 1 Nissl-stained coronal sections showing the nucleus accumbens in capuchin (**A**, **D**), macaque (**B**, **E**), and chimpanzee (**C**, **F**). The regions outlined in **A**, **B**, and **C** are shown at higher resolution in **D**, **E**, and **F**, respectively. The NAcc sampled was conservatively estimated to avoid sampling within the ventral striatum, as the border between these regions is indistinct. *ac* anterior commissure, *C* caudate nucleus, *cc* corpus callosum, *ic* internal capsule, *P* putamen, *NAcc* nucleus accumbens. Scale bar = 1 cm for panels **A**, **B**, and **C**

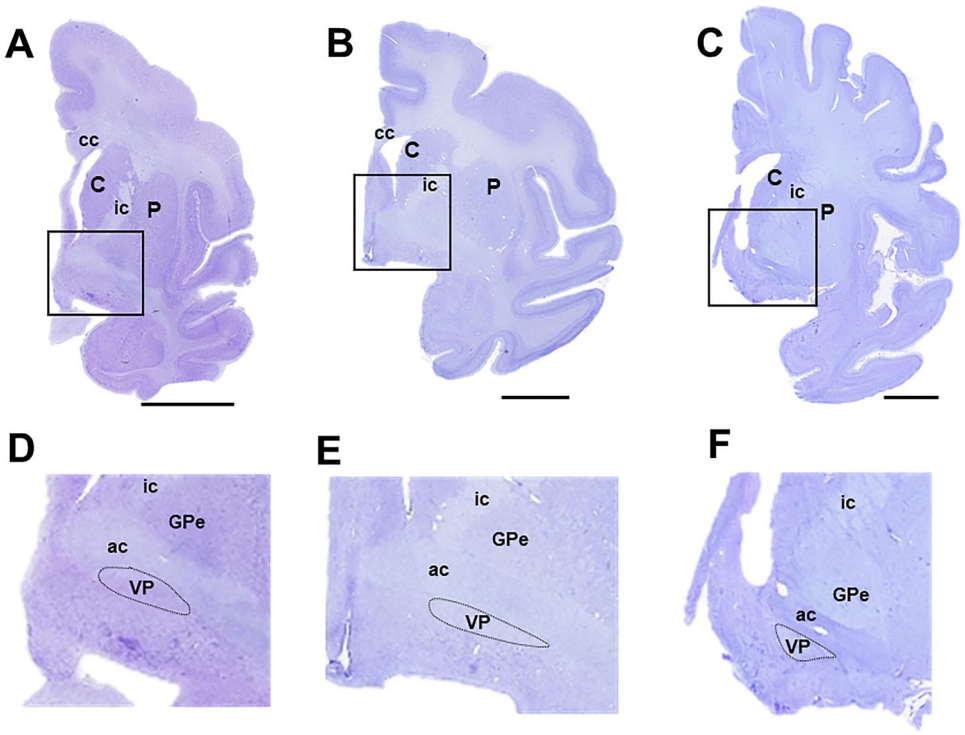

Fig. 2 Nissl-stained coronal sections showing the ventral pallidum (VP) in capuchin (**A**, **D**), macaque (**B**, **E**), and chimpanzee (**C**, **F**). The regions outlined in **A**, **B**, and **C** are shown at higher resolution in **D**, **E**, and **F**, respectively. *ac* anterior commissure, *C* caudate nucleus; cc, corpus callosum, *ic* internal capsule, *GPe* external globus pallidus, *P* putamen, *VP* ventral pallidum. Scale bar = 1 cm for panels **A**, **B**, and **C**

Sampling grids were optimized for each specimen, with an average grid of 496 × 401 µm (range 106 × 66–1632 × 1092). Axons were marked, where they intersected the outline of the hemisphere. Axon length density (ALv) was calculated as the total fiber length (µm) divided by the planimetric measurement (µm^3) of the reference volume sampled. Based on subsampling results, three sections per region per individual were quantified to reliably provide coefficients of error of less than 0.10. The section sampling interval ranged from 1 in 5 for smaller brains to 1 in 20 for larger brains. The mean number of sampling sites in the NAcc per individual was 29 ± 5 (s.d.) with an average of 131 ± 38 axon intersections counted per region. The mean number of sampling sites in the VP per individual was 28 ± 6 with an average of 72 ± 40 axon intersections counted per region. The Gundersen coefficient of error (CE, $m = 1$) was 0.06 ± 0.03.

Neuron density (Nv) and glial density (Gv) were assessed in adjacent Nissl-stained sections using the optical fractionator probe. While neuron densities were quantified for the purpose of standardizing the comparative data, glia densities were also collected at the same time. The ratio of glia to neurons (G/N) has been used to examine cell type composition across species and brain region (Sherwood et al. 2006). Nv and Gv are reported as the estimated population divided by the planimetric volume (µm^3). The NAcc and VP were outlined at 4× magnification and neurons and glia were manually counted under a 40× objective (N.A. 0.75) with a counting frame of 50 × 50 µm. As there is a significantly large range in the size of the specimens in this comparative sample, sampling grids also varied in size with an average of 550 × 459 µm (range 78 × 111–1280 × 1702). The optical disector height was 7 µm with a 2% guard zone. Section thickness was measured at every 5th sampling site and the average mounted section thickness for Nissl-stained sections was 13.4 ± 4.9 µm. The Gundersen CE ($m = 1$) was 0.07 ± 0.003 for Nv and 0.06 ± 0.01 for Gv. Neurons were identified by the presence of a large, lightly stained nucleus and a distinct nucleolus, accompanied by lightly stained dendritic processes. Glia cells do not possess a visible nucleolus or dendritic processes. Due to the difficulty in differentiating astrocytes, oligodendrocytes, and microglia in Nissl-stained sections, all glia were included. Nv and Gv were calculated as the sum of neurons or glia counted, respectively, within the sum of optical disectors divided by the product and volume of the disector (e.g., Sherwood et al. 2006).

Because the specimens included in this study are derived from species with vastly different brain sizes, we used the ratio of ALv/Nv for comparative analysis among species. Using neuron density as a denominator provides a variable that accounts for the fact that axons are innervating neurons regardless of brain size. In addition, glia densities (Gv) and glia-to-neuron ratios were evaluated for each region across species.

Statistical analysis

We used IBM SPSS software, TIBCO Statistica Academic and R to analyze the data. Among-species differences were evaluated using analysis of variance (ANOVA) in the NAcc and VP separately. The dependent variables were TH ALv/Nv, Nv, Gv, and glia-to-neuron ratio (G/N). A Brown–Forsythe correction was applied when Levene's test for homogeneity of variance was significant. Significant results were evaluated using Fisher's least significant difference (LSD) post hoc tests. Prior to among-species analyses, separate independent sample *T* tests were used to test for differences between sexes in each species. The results from these analyses were non-significant ($p > 0.05$ for all); therefore, sexes were pooled.

Additional analyses to determine allometric scaling relationships with brain weight were performed using R studio software (R core Team, Vienna, Austria, version 4.0.2). Species mean data were evaluated using phylogenetic generalized least squares (PGLS) to calculate scaling slopes while accounting for the covariance structure of evolutionary relatedness. In these analyses, *Aotus* spp. individuals were pooled with *Aotus trivirgatus*. Phylogenetic analysis of covariance (pANCOVA) was used to test whether human values were significantly different from what would be expected for their brain size (Smaers and Rohlf 2016). PGLS and pANCOVA were performed for NAcc and VP data separately. The dependent variables were TH ALv/Nv, Nv, Gv, and glia-to-neuron (G/N) ratio, while the independent variable was brain weight. The level of significance (α) was set at 0.05 for all statistical tests.

Results

Among-species analyses

TH ALv/Nv

Figures 3, 4, 5 and 6 provide examples of TH immunohistochemical staining of the NAcc and VP for all species. Immunostaining was robust for all individuals used in this study. Notably, there are differences among species and between regions for the number and size of TH-ir

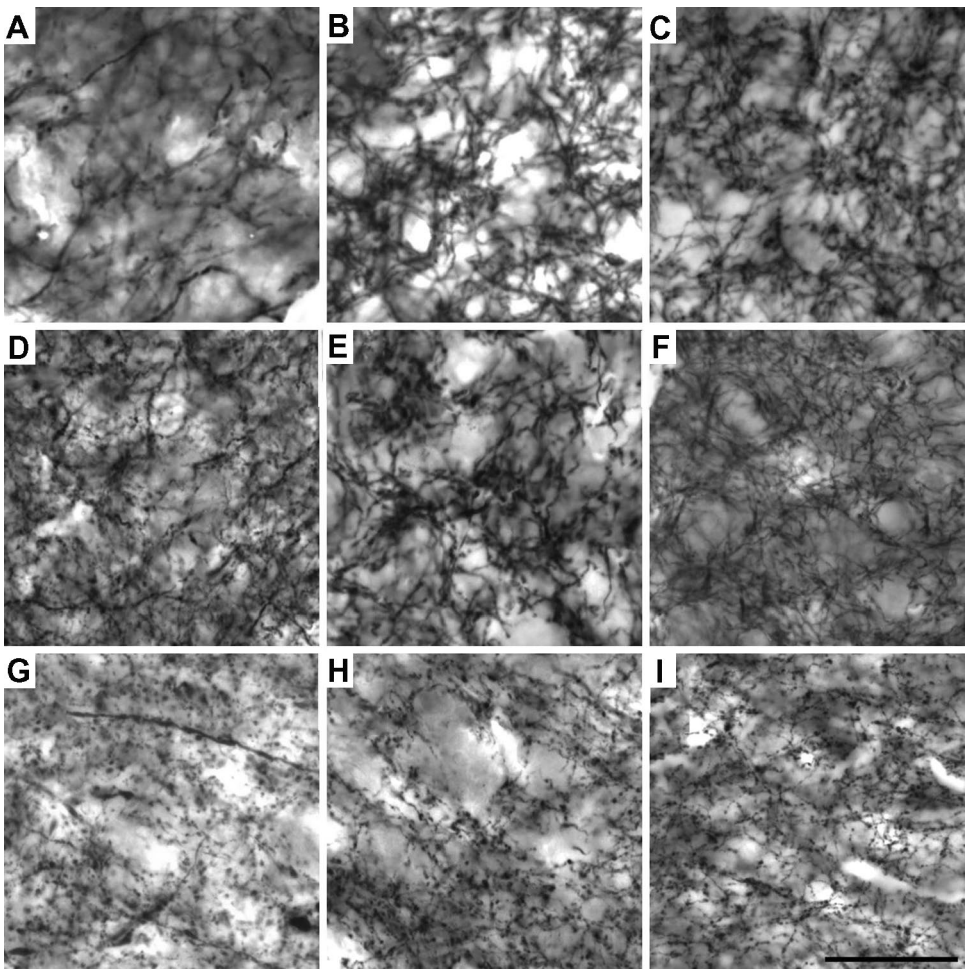

Fig. 3 High-magnification photomicrographs of TH-ir axons in the NAcc in marmoset (**A**), tamarin (**B**) owl monkey (**C**), capuchin (**D**), rhesus macaque (**E**), pig-tailed macaque (**F**), chimpanzee (**G**), bonobo (**H**), and human (**I**). Scale bar in I = 25 µm

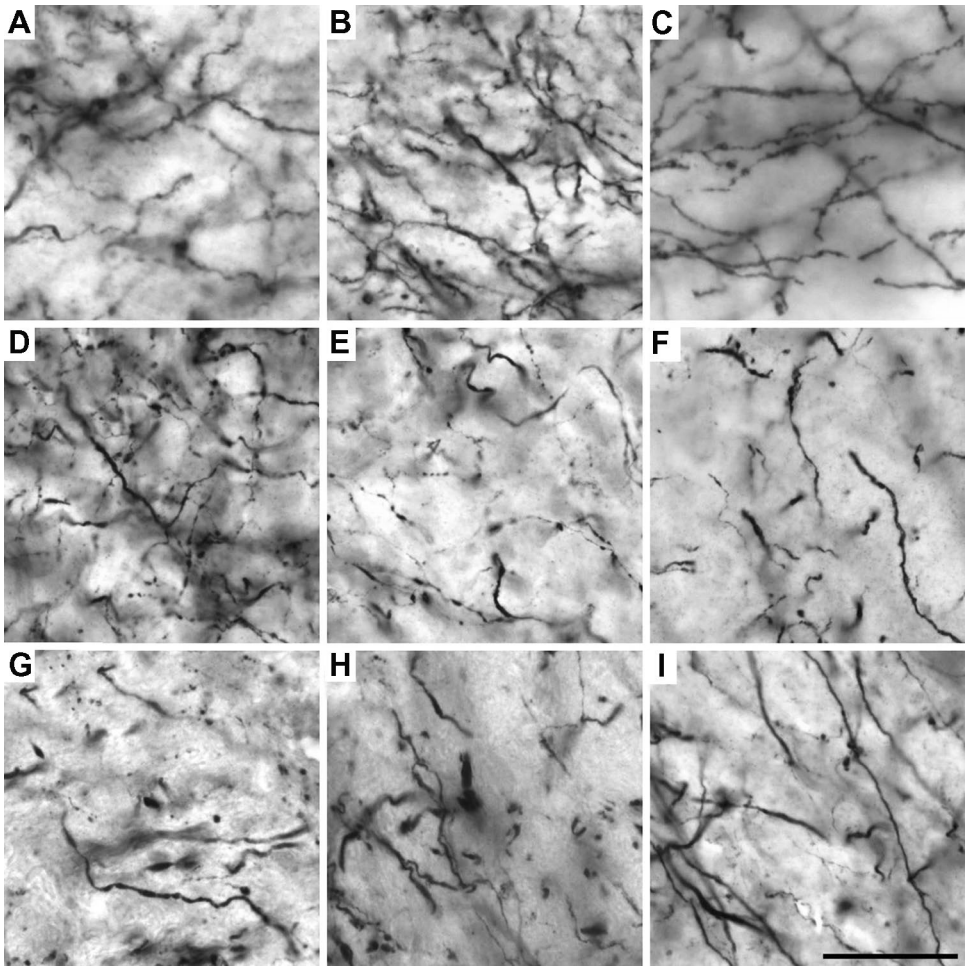

Fig. 4 High-magnification photomicrographs of TH-ir axons in the VP in marmoset (**A**), tamarin (**B**), owl monkey (C), capuchin (**D**), rhesus macaque (**E**), pig-tailed macaque (**F**), chimpanzee (**G**), bonobo (**H**), and human (**I**). Scale bar in I = 25 µm

varicosities and axons. Generally speaking, axons were finer and with a higher concentration of smaller varicosities in the NAcc. TH-ir axons within the VP were thicker with larger, although more widely spaced, varicosities. Tables 2 and 3 provide summary data for all variables by species. ANOVA analysis revealed a significant difference among species for TH ALv/Nv in the NAcc ($F_{8,40} = 6.25$, $p < 0.025$; Fig. 7). Post hoc analyses indicated that humans possess significantly higher TH ALv/Nv in the NAcc relative to all nonhuman primate species ($p < 0.05$ for all). Our next analysis used PGLS to examine allometric scaling of TH ALv/Nv against brain weight while accounting for phylogenetic relatedness in the comparative sample. The PGLS regression indicated a significant positive scaling relationship across the primates between TH ALv/Nv and brain weight for the NAcc ($df = 10$, regression slope $b = 0.24$, 95% CI 0.13–0.35, $p = 0.0006$; Fig. 8). pANCOVA demonstrated that human TH ALv/Nv in the NAcc was significantly higher than expected from the overall primate scaling trend ($df = 3$, $F = 7.73$, $p = 0.021$).

TH ALv/Nv in the VP was also significantly different among species ($F_{8,38} = 5.35$, $p < 0.025$; Fig. 7), with humans having significantly higher ALv/Nv than nonhuman primate species ($p < 0.05$ for all). PGLS analysis showed that TH ALv/Nv in the VP displayed a significant positive scaling relationship ($df = 10$, regression slope $b = 0.26$, 95% CI 0.17–0.36, $p = 0.0001$; Fig. 8). Human TH ALv/Nv in the VP was relatively high, with pANCOVA finding the human value approaching a conventional level for statistical significance in deviating from primate scaling predictions ($df = 3$, $F = 3.84$, $p = 0.082$).

Neurons and Glia

NAcc Nv results revealed a significant difference among species ($F_{8,40} = 4.60$, $p < 0.025$; Fig. 7). Post hoc analyses indicated that marmosets possessed significantly higher neuron density than all other species. Humans possessed significantly lower neuron density compared to tamarins, bonobos, and owl monkeys. A significant effect of species was also detected for VP Nv ($F_{8,38} = 7.98$, $p < 0.025$; Fig. 7). Post hoc analyses showed that marmosets have higher neuron densities relative to all species except owl monkeys (all p values < 0.05). Owl monkeys have higher

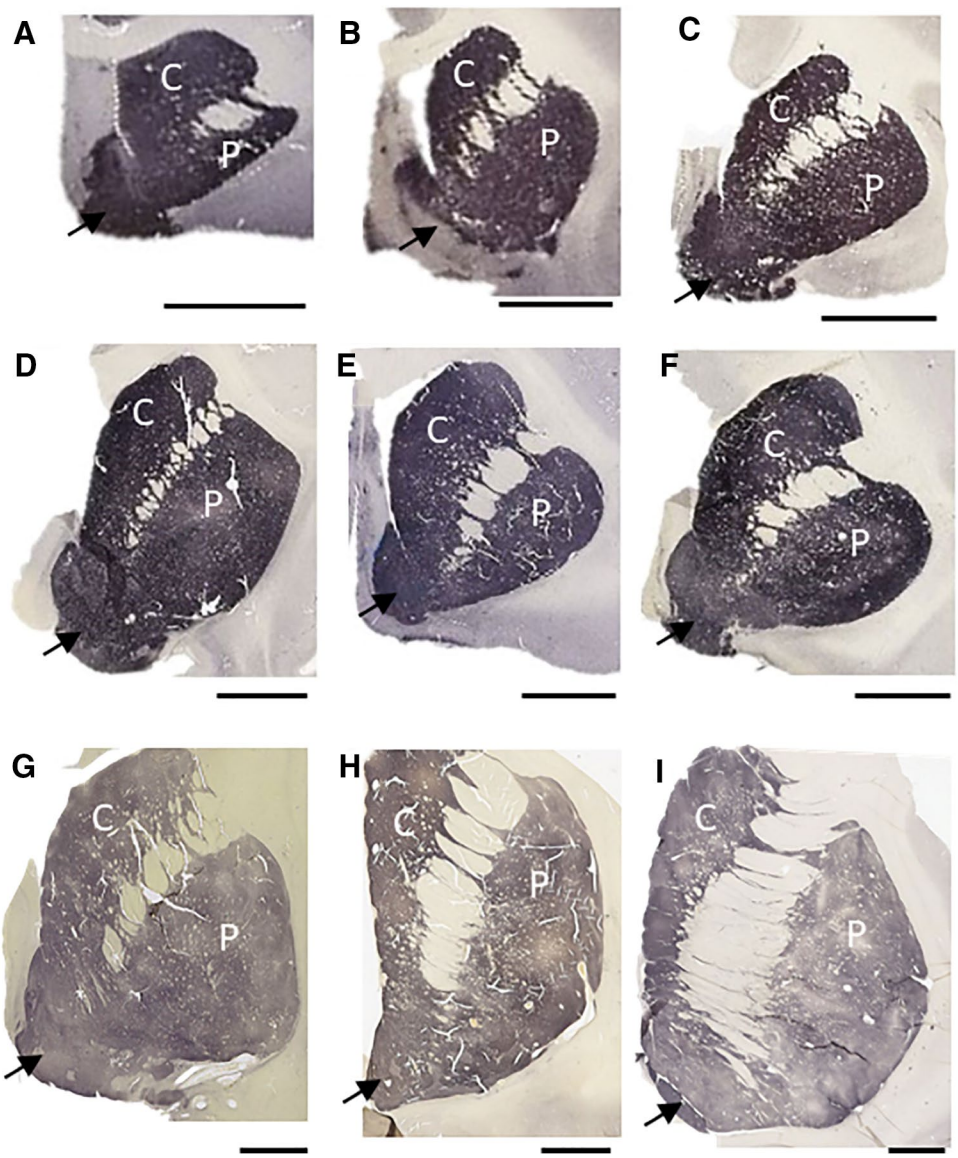

Fig. 5 Low-power photomicrographs showing TH-immunostained sections containing the NAcc. The NAcc is indicated by arrows. Note that there is not an obvious distinction between the shell and core regions of the NAcc. *C* caudate nucleus, *P* putamen. Scale bars = 0.5 cm

densities relative to capuchins and all catarrhines (all p values < 0.05). Tamarins display significantly increased neuron density compared to pig-tailed macaques, bonobos, and humans. Capuchins exhibit a significantly lower neuron density than did other platyrrhines. No differences were detected among catarrhines (all p values > 0.05). Interestingly, a species difference was not detected for NAcc Gv ($F_{8,40} = 1.348$, $p > 0.025$; Fig. 7) or VP Gv ($F_{8,38} = 1.790$, $p > 0.025$; Fig. 7).

NAcc G/N ratio analyses revealed significant differences among species ($F_{8,40} = 3.233$, $p < 0.025$; Fig. 7). Post hoc analyses indicated that humans displayed a significantly higher G/N ratio than all other species except capuchins. Capuchins had a significantly higher G/N ratio than all other platyrrhine monkeys. VP G/N analyses were significantly different among species ($F_{8,38} = 4.28$, $p < 0.025$; Fig. 4). Humans possess a significantly higher G/N ratio than all other species except pig-tailed macaques and bonobos. Both species display a higher G/N ratio compared to all platyrrhines.

PGLS analyses (Fig. 9) indicated significant negative scaling between Nv and brain weight in the NAcc ($df = 10$, regression slope $b = -0.19$, 95% CI −0.31 to −0.07, $p = 0.0062$) and the VP ($df = 10$, regression slope $b = -0.29$, 95% CI −0.42 to −0.15, $p = 0.0009$). In contrast, there was no relationship between Gv and brain weight in the NAcc ($df = 10$, regression slope of $b = 0.02$, 95% CI −0.08 to 0.13, $p = 0.6374$) or the VP ($df = 10$, regression slope $b = -0.07$, 95% CI −0.16 to 0.02, $p = 0.0964$). The G/N ratios in each region, consequently, displayed positive allometric scaling: NAcc ($df = 10$, regression slope $b = 0.40$, 95% CI 0.23–0.57, $p = 0.0003$)

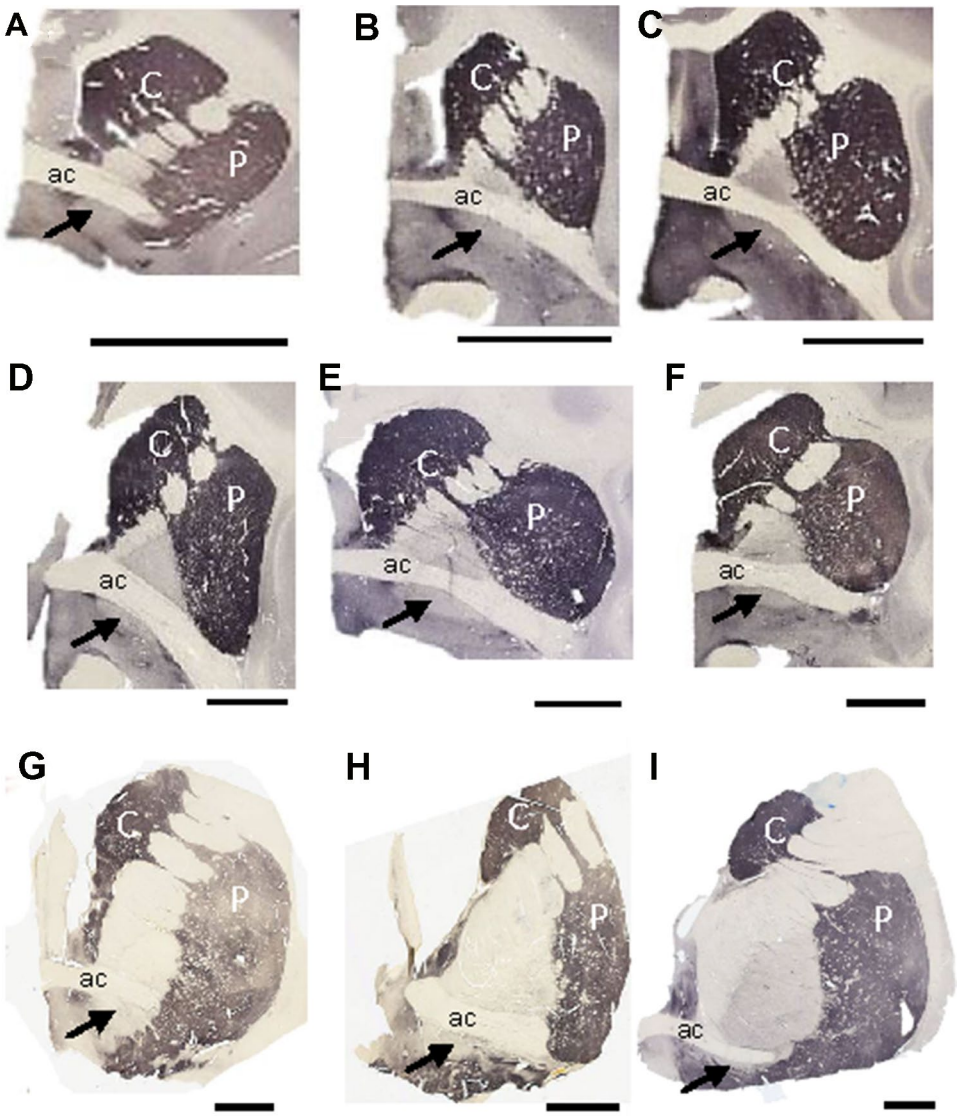

Fig. 6 Low-power photomicrographs showing TH-immunostained sections containing the VP. The VP is indicated by arrows and is easily identifiable in all sections with its distinct borders. *C* caudate nucleus, *P* putamen, *ac* anterior commissure. Scale bars = 0.5 cm

Table 2 Summary data for TH axon length density (ALv), neuron density (Nv), TH ALv/Nv, glia density (Gv), and glia to neuron ratio (G/N) for each species in the nucleus accumbens (NAcc)

Genus	TH ALv (μm/μm^3)	Nv (neurons/μm^3)	TH ALv/Nv	Gv (glia/μm^3)	G/N
Callithrix spp.	35,359,503 ± 13,126,716	159,788 ± 81,939	241.29 ± 90.13	133,260 ± 73,634	.85 ± .15
Saguinus oedipus	20,456,808 ± 6,463,875	94,391 ± 25,711	229.34 ± 99.55	88,419 ± 20,584	1.02 ± .43
Aotus spp.	30,569,387 ± 7,253,895	101,139 ± 51,251	337.91 ± 109.9	84,868 ± 48,672	.81 ± .10
Cebus apella	29,610.015 ± 15,075,605	61,559 ± 44,520	467.69 ± 167.4	137,895 ± 41,112	3.00 ± 1.76
Macaca mulatta	17,766,455 ± 7,115,746	67,524 ± 22,498	256.58 ± 84.69	110,359 ± 35,704	2.01 ± 1.44
Macaca nemestrina	17,355,095 ± 7,203,398	51,287 ± 20,536	363.78 ± 172.9	82,575 ± 15,091	1.74 ± .51
Pan troglodytes	26,979,932 ± 2,958,398	77,714 ± 14,057	352.70 ± 47.35	96,138 ± 52,820	1.24 ± .62
Pan paniscus	47,311,086 ± 13,961,461	94,127 ± 30,620	526.67 ± 135.1	120,157 ± 55,220	1.30 ± .40
Homo sapiens	38,852,153 ± 10,445,364	38,804 ± 17,699	1242.2 ± 801.5	133,250 ± 47,120	4.43 ± 3.73

Table 3 Summary data for TH axon length density (ALv), neuron density (Nv), TH ALv/Nv, glia density (Gv), and glia to neuron ratio (G/N) for each species in the ventral pallidum (VP)

Genus	TH ALv (μm/μm^3)	Nv (neurons/μm^3)	TH ALv/Nv	Gv (glia/μm^3)	G/N
Callithrix spp.	38,424,091 ± 35,379,311	82,282 ± 43,706	502.97 ± 545.66	207,626 ± 91,768	2.49 ± .27
Saguinus oedipus	19,557,066 ± 4,767,129	51,120 ± 8,495	391.60 ± 112.07	162,862 ± 41,059	3.23 ± .83
Aotus spp.	25,716,375 ± 8,383,588	69,253 ± 25,266	374.53 ± 17.37	150,104 ± 78,724	2.08 ± .66
Cebus apella	19,984,428 ± 8,288,468	33,029 ± 9,107	598.78 ± 169.3	141,935 ± 35,705	4.39 ± .84
Macaca mulatta	14,832,980 ± 4,566,302	31,472 ± 4,827	468.96 ± 103.66	167,385 ± 47,208	5.25 ± .83
Macaca nemestrina	11,345,480 ± 2,104,688	15,333 ± 4,712	783.93 ± 215.62	101,138 ± 20,833	6.87 ± 1.52
Pan troglodytes	12,877,586 ± 1,564,131	32,984 ± 22,449	515.25 ± 252.51	118,253 ± 34,197	5.21 ± 4.20
Pan paniscus	11,379,280 ± 3,935,412	19,540 ± 7,938	615.71 ± 171.88	139,552 ± 44,864	7.84 ± 2.66
Homo sapiens	24,707,901 ± 10,494,620	20,522 ± 12,709	1579.37 ± 817.6	145,732 ± 62,153	9.44 ± 6.05

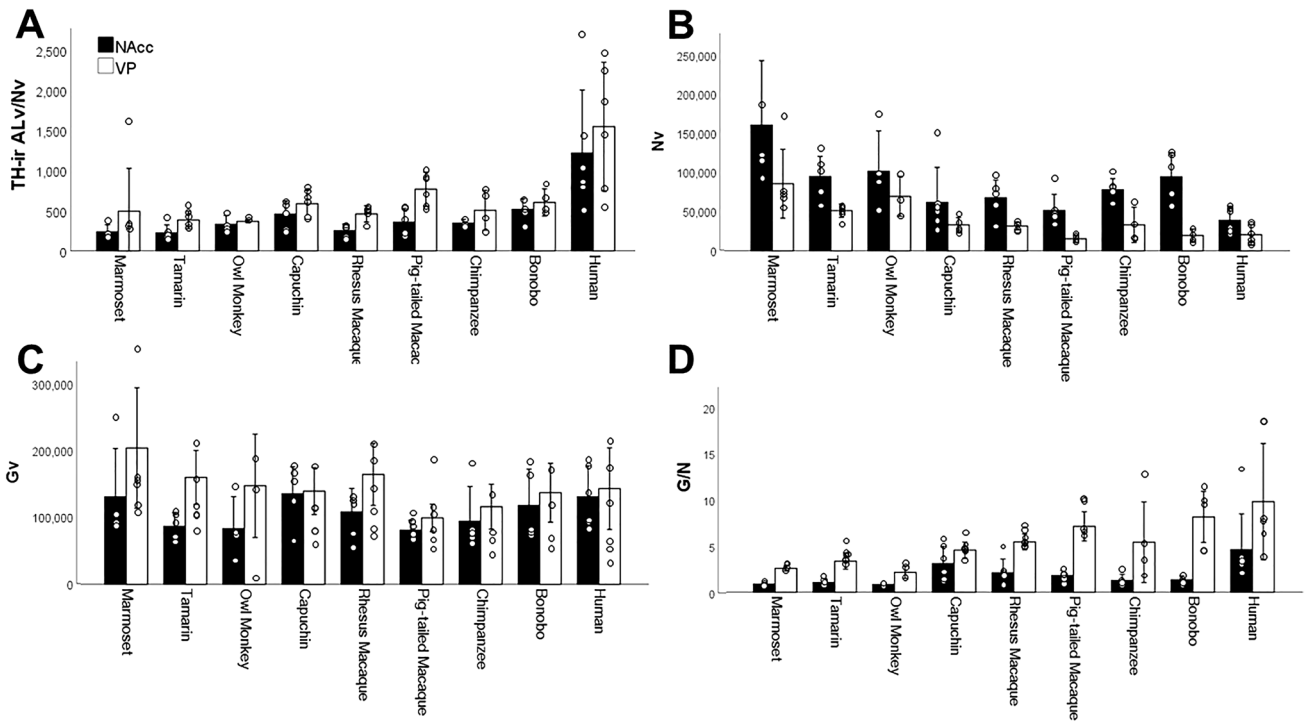

Fig. 7 Bar graphs showing mean TH-ir ALv/Nv (TH-ir positive axon length density/neuron density; **A**), Nv (estimated neuron population/planimetric volume in μm^3; **B**), Gv (estimated glia population/planimetric volume in μm^3; **C**), and glia to neuron (G/N) ratio (**D**) in the NAcc and VP by species. The open circles represent individual values. Error bars show ± 1 SD

and VP ($df = 10$, regression slope of $b = 0.21$, 95% CI 0.11–0.32, $p = 0.001$). pANCOVA analysis indicated that humans do not differ from the overall primate trend in neuron and glia densities of NAcc and VP, or for G/N ratio in VP. However, the human G/N ratio in the NAcc did depart significantly from the overall primate trend in being elevated ($df = 3$, $F = 6.35$, $p = 0.033$).

Discussion

DA transmission in the ventral striatum, and specifically in the NAcc, plays a major role in behavioral flexibility. It is important to note that in many studies, the ventral striatum and NAcc are treated as the same structure although there are clear distinctions between the two regions (e.g., Haber and McFarland 1999; Haber et al. 2006). The ability to

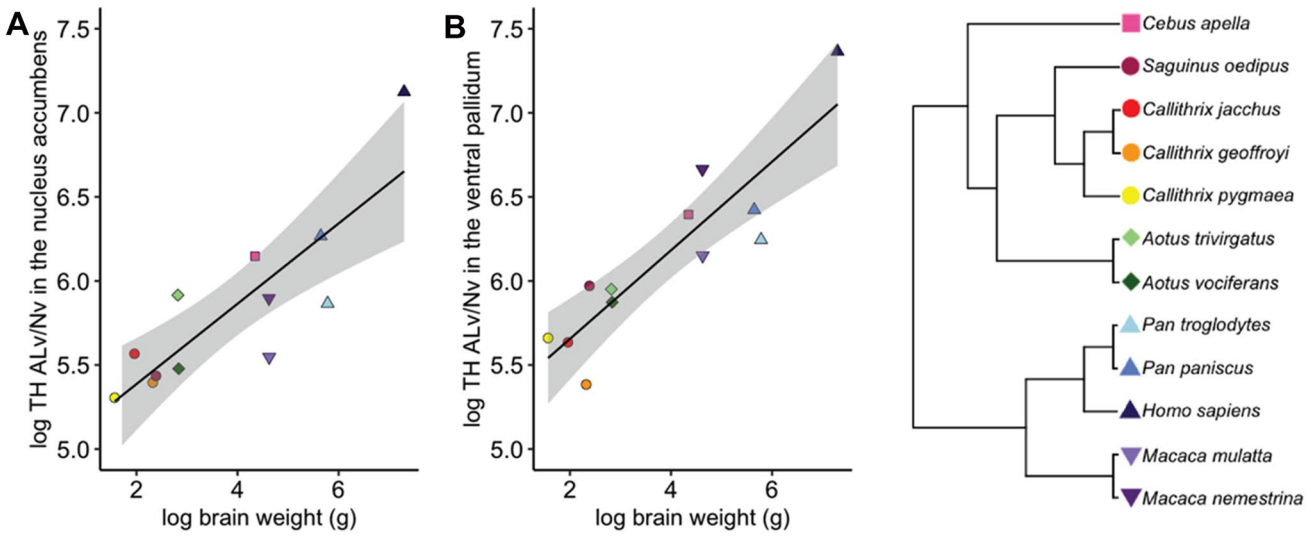

Fig. 8 PGLS regressions of TH AL/Nv (TH-ir positive axon length density/neuron density) against brain weight shown with 95% confidence intervals for nucleus accumbens (**A**) and ventral pallidum (**B**). The phylogenetic tree in this figure provides the color/shape legend for species values in all plots of PGLS analyses

evaluate different levels of reward, especially those involving value versus risk, as well as simultaneously reducing the likelihood of adverse outcomes, are essential components of developing goal-directed behavior, especially in the context of group living (Haber 2014). DA released from the VTA into the NAcc mediates incentive salience, especially the motivation to behave in a particular way in response to certain stimuli (Báez-Mendoza et al. 2013; Báez-Mendoza and Schultz 2013). Although the roles of DAergic pathways in modulating cognition, social behavior, and personality in both human and other primates are yet to be fully explored, these systems likely impact social organization, reproductive strategies, and foraging patterns.

Here, we present the results of a comparative analysis of DAergic innervation, Nv, Gv, and G/N ratios in the NAcc and VP in a large sample of haplorrhine primates, including humans. Consistent with previous reports that examined other brain regions in comparative samples of mammals, we found an inverse relationship between neuron density and brain weight and no correlation of glia density with brain size (e.g., Haug 1987; Herculano-Houzel 2014; Sherwood et al. 2006; see Fig. 9). G/N ratios increased allometrically with brain weight in both areas and these scaling patterns were similar to what has been reported for cortex. Interestingly, humans possessed a significantly increased G/N ratio within the NAcc relative to the other primates in our sample (see Fig. 7). This resulted from a combination of both decreased neuron density and increased glia density within this region. Classically, the G/N ratio has been considered to be a measure of metabolic support (Hawkins and Olszewski 1957); however, it is possible that developmental constraints and variation in neuron size may drive inter-species differences (Herculano-Houzel 2014).

Humans were also distinguished in having significantly higher DAergic innervation in both the VP and NAcc compared to other primates (see Figs. 7 and 8), even while accounting for overall brain size and phylogenetic relatedness in our comparative sample. This pattern is consistent with the uniquely human neurochemical profile previously reported for the dorsal striatum, suggesting evolutionary reorganization of the human striatum (Raghanti et al. 2018). This unique striatal neurochemistry includes increases in TH-containing neurons and axons in the dorsal and middle caudate nucleus, and differential expression of multiple DA-related genes compared to those in rodents and nonhuman primates (Inoue-Murayama et al. 2002; Miller and Madras 2002; Raghanti et al. 2018; Sousa et al. 2017). The increased G/N ratio of human NAcc, a region critical to the brain's reward pathway, combined with greater DAergic innervation, may prove to have played a significant role in our unique vulnerability to addiction and psychiatric disorders, including depression and anxiety (Calvey 2019; Mavridis 2015).

We originally anticipated that humans and other monogamous and semi-monogamous primates would share increased DA within one or both regions of interest based on previous studies conducted in rodent species (Aragona et al. 2006; Curtis et al. 2006). However, owl monkeys, marmosets, and tamarins did not exhibit increased DA relative to non-monogamous species in our study. While this deviates from what we expected from work conducted in prairie voles, it is consistent with what has been reported for titi monkeys (*Callicebus cupreus*). Hostetler (2017)

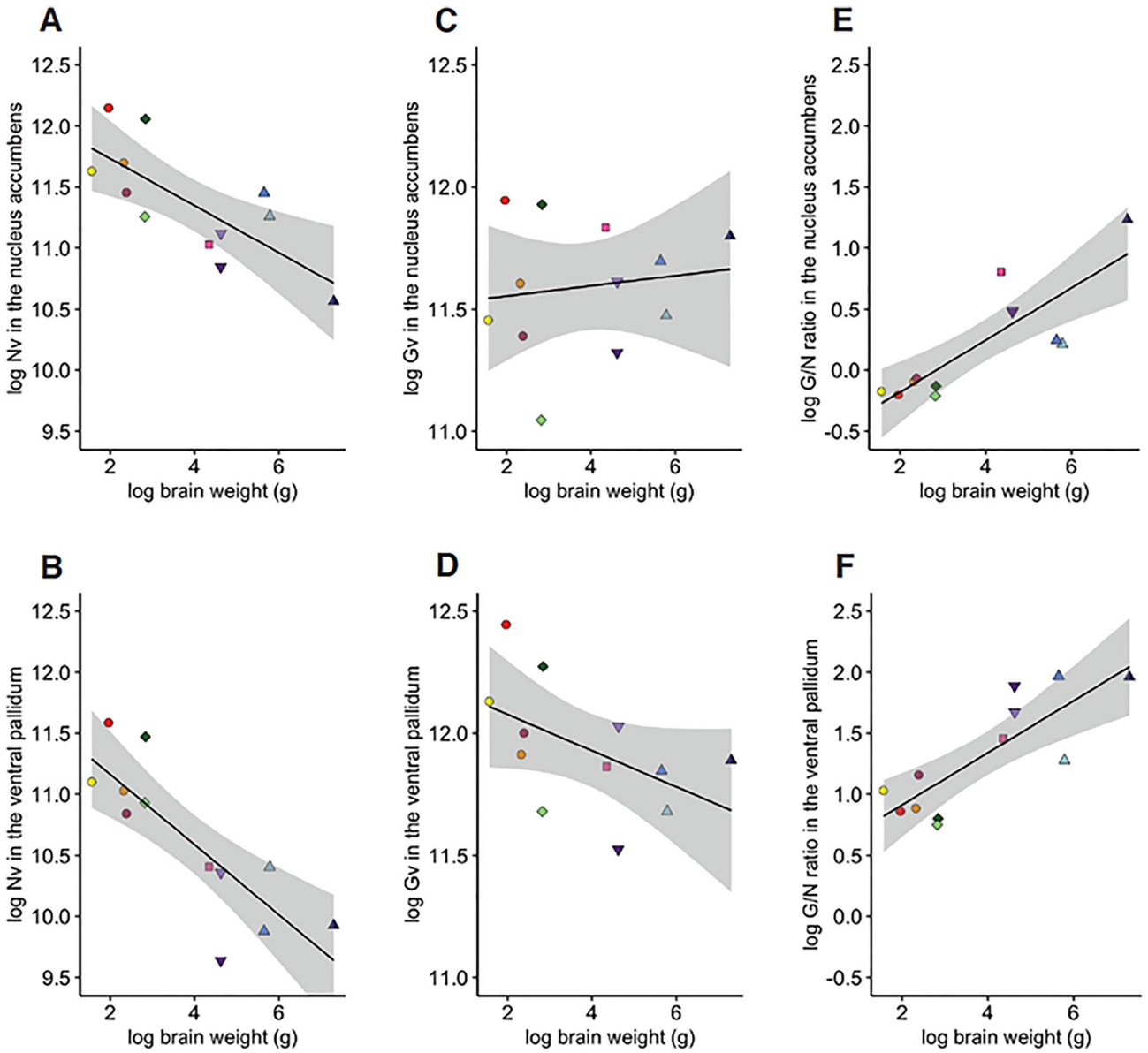

Fig. 9 PGLS regressions against brain weight shown with 95% confidence intervals for Nv (estimated neuron population/planimetric volume in μm^3) in the nucleus accumbens (**A**) and ventral pallidum (**B**), Gv (estimated glia population/planimetric volume in μm^3), in the nucleus accumbens (**C**) and ventral pallidum (**D**), and G/N ratio in the nucleus accumbens (**E**) and ventral pallidum (**F**). The phylogenetic tree in this figure provides the color/shape legend for species values in all plots of PGLS analyses

examined DA binding (to the D1 receptor) in male titi monkeys after their pairing with a female and found an increase in the lateral septum, but not in the NAcc or other regions implicated in the prairie vole model of monogamy. While features of the neuroanatomical substrates that regulate monogamy are likely conserved among mammals (Young and Wang 2004), these results highlight the need for further development of nonhuman primate and other models for gaining a more comprehensive understanding of how neurobiology modulates behaviors across species (Phillips et al. 2014; Preuss 2019). In particular, our ability to distinguish whether monogamous marmosets, tamarins, and owl monkeys display a particular DAergic profile in the NAcc and ventral pallidum would have been improved if we had additional non-monogamous platyrrhine primates besides capuchins for our outgroup comparisons. Furthermore, inclusion of monogamous primate species phyletically closer to humans (e.g., gibbons and siamangs) may provide additional resolution.

We previously argued that a change in neurochemistry, including a more DA-dominated striatum, may have been pivotal in the evolution of the human lineage by supporting

an increased sensitivity to social and environmental cues as well as decreased within-group aggression (Raghanti et al. 2018). Such changes may have been coincident with the emergence of bipedality and the reduction of the canine (the social tooth) > 4 million years ago (e.g., Holloway 1967; Lovejoy 2009). The sectorial canine complex refers to the continual honing of the upper canine's critical shearing capacity that maintains it as a potential weapon (e.g., Holloway 1967; Lovejoy 2009). The striatum plays a major role in social behaviors, particularly those involved in social reward (e.g., Baez-Mendoza et al. 2013). Research in nonhuman primates, rodents, and cats has demonstrated that relative activity levels of dorsal versus ventral striatal regions contributes to individual personality style (e.g., exploratory behaviors, sensitivity to social and environmental cues, extraversion, etc.) (see van den Bos 2015; Van der Bercken and Cools 1982 for reviews). Individuals with increased relative activity in the dorsal striatum were more internally motivated with a high degree of autonomy and a more superficial knowledge of their environment, and were more aggressive, dominant, and less responsive to social events. Individuals with increased activity in the ventral striatum were less aggressive and more externally driven, with a greater interest in their environment. They were also highly responsive to social stimuli (reviewed in van den Bos 2015; Van der Bercken and Cools 1982).

Striatal neurochemistry has been linked to behaviors that are associated with these 'personality styles', including exploratory behaviors, sensitivity to social and environmental cues, and extraversion (e.g., Bergey et al. 2016; Cools et al. 1975; Jolly et al. 2008; Jolly et al. 2013; Higley et al. 1996; Raleigh et al. 1991; Rilling and Sanfey, 2011; Tanaka et al. 2004; Tanaka et al. 2007; Van den Bercken and Cools 1982). Increased DA shifts activity to the ventral striatum and its associated personality style, while decreased DA shifts activity to the dorsal striatum and its associated behaviors. Individual variation in personality styles and their effects on potential cooperative interaction could have been targets of selection in early human ancestral populations. Enhanced awareness of habitat, decreased aggression, and elevated social conformity are all associated with a DA-dominated striatum personality style, and each could have improved survivorship and reproductive success, thus ultimately undergoing strong selection (Raghanti et al. 2018). Moreover, further expansion of this personality style may have provided the cognitive flexibility and social intelligence underlying not only acquisition of language and speech, but also a strong tendency towards social conformity, altruism, and empathy—the suite of extraordinary characters that have come to define human uniqueness.

While personality style and social behaviors can be linked to current experimental data from primate and rodent species, it is important to note that these postmortem analyses cannot definitively link specific cognitive or behavioral characteristics with innervation patterns. This level of interpretation will require future research to allow a more complete understanding of the neuroanatomical bases of human versus nonhuman behaviors.

Acknowledgements This research was funded by the National Science Foundation (NSF BCS-1846201 to MAR and SMA-1542848 and EF-2021785 to CCS and WDH). Elaine Miller was supported by the National Science Foundation Graduate Research Fellowship Program (1746914). We would like to thank Dr. Richard S. Meindl for statistical advice. We are grateful to each of the following for the use of brain materials: The NIH NeuroBioBank, National Chimpanzee Brain Resource (NIH grant NS092988), NINDS Grants NS-402867 and NS0-73134, The Great Ape Aging Project (supported by NIH Grant AG014308), the National Primate Research Center at the University of Washington (NIH grant RR000166), the Oregon National Primate Research Center (NIH P51 OD011092), the Northwestern University Alzheimer's Disease Center Brain Bank (supported by Alzheimer's Disease Core Center Grant AG013854, from the National Institute on Aging to Northwestern University, Chicago, IL).

Author contributions KH and MAR contributed to the study conception and design. Material preparation, data collection and analysis were performed by KH, EM, CDS, KAP, WDH, PRH, CCS, COL, and MAR. The first draft of the manuscript was written by KH and MAR and all authors commented on previous versions of the manuscript. All authors read and approved the final manuscript.

Funding This research was funded by the National Science Foundation (NSF BCS-1846201 to MAR and SMA-1542848 and EF-2021785 to CCS and WDH). Elaine Miller was supported by the National Science Foundation Graduate Research Fellowship Program (1746914).

Availability of data and materials All raw data are available and will be posted in the National Chimpanzee Brain Resource website data repository (https://www.chimpanzeebrain.org/data-repository) and can be requested from the corresponding authors.

Code availability NA.

Declarations

Conflict of interest None.

Ethics approval Human postmortem brain samples meet the criteria for IRB Exemption 4 under DHHS regulations 45 CFR 46 (46.101). Because no living subjects are involved in this research, this proposal does not qualify for IACUC oversight. However, when alive, all nonhuman primates were housed at research or zoological institutions and were maintained in accordance with each institution's animal care and use guidelines.

Consent to participate NA.

Consent for publication NA.

References

Aragona BJ, Liu Y, Yu YJ, Curtis JT, Detwiler JM, Insel TR, Wang Z (2006) Nucleus accumbens dopamine differentially mediates the formation and maintenance of monogamous pair bonds. Nature Neurosci 9:133–139

Arias-Carrión O, Stamelou M, Murillo-Rodriguez E, Menéndez-González M, Pöppel E (2010) Dopaminergic reward system: a short integrative review. Int Arch Med 3:24

Báez-Mendoza R, Schultz W (2013) The role of the striatum in social behavior. Front Neurosci 7:233

Báez-Mendoza R, Harris CJ, Schultz W (2013) Activity of striatal neurons reflects social action and own reward. Proc Nat Acad Sci USA 110:16634–16639

Bales KL, Mason WA, Catana C, Cherry SR, Mendoza SP (2007) Neural correltaes of pair-bonding in a monogamous primate. Brain Res 1184:245–253

Bergey CM, Phillips-Conroy JE, Disotell TR, Jolly CJ (2016) Dopamine pathway is highly diverged in primate species that differ markedly in social behavior. Proc Natl Acad Sci USA 113:6178–6181

Calvey T (2019) Human self-domestication and the extended evolutionary synthesis of addiction: how humans evolved a unique vulnerability. Neuroscience 419:100–107

Cools AR, Hendriks G, Korten J (1975) The acetylcholine-dopamine balance in the basal ganglia of rhesus monkeys and its role in dynamic, dystonic, dyskinetic, and epileptoid motor activities. J Neural Transm 36:91–105

Cools AR, Brachten R, Heeren D, Willemen A, Ellenbroek B (1990) Search after neurobiological profile of individual-specific features of Wistar rats. Brain Res Bull 24:49–69

Curtis JT, Liu Y, Aragona BJ, Wang Z (2006) Dopamine and monogamy. Brain Res 1126:76–90

Filkowski MM, Cochran RN, Haas BW (2016) Altruistic behavior: mapping responses in the brain. Neurosci Neuroecon 5:65–75

Haber SN (2003) The primate basal ganglia: parallel and integrative networks. J Chem Neuroanat 26:317–330

Haber SN (2014) The place of dopamine in the cortico-basal ganglia circuit. Neuroscience 282:248–257

Haber SN, Knutson B (2010) The reward circuit: linking primate anatomy to human imaging. Neuropsychopharmacology 35:4–26

Haber SN, McFarland NR (1999) The concept of the ventral striatum in nonhuman primates. Ann NY Acad Sci 877:33–48

Haber SN, Kunishio K, Mizobuchi M, Lynd-Balta E (1995) The orbital and medial prefrontal circuit through the primate basal ganglia. J Neurosci 15:4851–4867

Haber SN, Kim K-S, Mailly P, Cazavara R (2006) Reward-related cortical inputs define a larger striatal region in primates that interface with associative cortical connections, providing a substrate for incentive-based learning. J Neurosci 26:8368–8376

Haug H (1987) Brain sizes, surfaces, and neuronal sizes of the cortex cerebri: a stereological investigation of man and his variability and a comparison with some mammals (primates, whales, marsupials, insectivores, and one elephant). Am J Anat 180:126–142

Hawkins A, Olszewski J (1957) Glia/nerve cell index for cortex of the whale. Science 126:76–77

Herculano-Houzel S (2014) The glia/neuron ratio: How it varies uniformly across brain structures and species and what it means for brain physiology and evolution. Glia 62:1377–1391

Higley JD, King ST Jr, Hasert MF, Champoux M, Suomi SJ, Linnoila M (1996) Stability of interindividual differences in serotonin function and its relationship to severe aggression and competent social behavior in rhesus macaque females. Neuropsychopharmacol 14:67–76

Holloway RL (1967) Tools and teeth: some speculations regarding canine reduction. Am Anthropol 69:63–67

Hostetler CM et al (2017) Effects of pair bonding on dopamine D1 receptors in monogamous male titi monkeys (*Callicebus cupreus*). Am J Primatol 79:e22612

Inoue-Murayama M et al (2002) Variation of variable number of tandem repeat sequences in the 3′-untranslated region of primate dopamine transporter genes that affects reporter gene expression. Neurosci Lett 334:206–210

Jolly CJ, Phillips-COnroy JE, Kaplan JR, Mann JJ (2008) Cerebrospinal fluid monoaminergic metabolites in wild *Papio anubis* and *P. hamadryas* are concordant with taxon-specific behavioral ontogeny. Int J Primatol 29:1549–1566

Jolly CJ, Phillips-Conroy JE, Kaplan JR, Mann JJ (2013) Monoamine neurotransmitter metabolites in the cerebrospinal fluid of a group of hybrid baboons (*Papio hamadryas and P. anubis*). Int J Primatol 34:836–858

Kalivas PW, Volkow ND (2005) The neural basis of addition: a pathology of motivation and choice. Am J Psychiatry 162:1403–1413

Klimecki OM, Leiberg S, Ricard M, Singer T (2014) Differential pattern of functional brain plasticity after compassion and empathy training. Soc Cogn Affect Neurosci 9:873–879

Klucharev V, Hytönen K, Rijpkema M, Smidts A, Fernández G (2009) Reinforcement learning signal predicts social conformity. Neuron 61:140–151

Lovejoy CO (1981) The origin of man. Science 211:341–350

Lovejoy CO (2009) Reexamining human origins in light of *Ardipithecus ramidus*. Science 326:74e71-74e78

Lovejoy CO (2014) *Ardipithecus* and early human evolution in light of twenty-first-century developmental biology. J Anthropol Res 70:337–363

Mavridis I (2015) The role of the nucleus accumbens in psychiaric disorders. Psychiatriki 25:282–294

McCollum LA, McCullumsmith RE, Roberts RC (2016) Tyrosine hydroxylase localization in the nucleus accumbens in schizophrenia. Brain Sruct Funct 221:4451–4458

Miller GM, Madras BK (2002) Polymorphisms in the 3'-untranslated region of human and monkey dopamine transporter genes affect reporter gene expression. Mol Psychiatry 7:44–55

Nowak RM (1999) Walker's primates of the world. The Johns Hopkins University Press, Baltimore

O'Connell LA, Hofmann HA (2011) The vertebrate mesolimbic reward system and social behavior network: a comparative synthesis. J Comp Neurol 519:3599–3639

Paxinos G et al (2000) The rhesus monkey brain in stereotaxic coordinates. Academic Press, San Diego, CA

Paxinos G, Watson C, Petrides M, Rosa M, Tokuno H (2012) The marmoset brain in stereotaxic coordinates. Academic Press/Elsevier

Phillips KA et al (2014) Why primate models matter. Am J Primatol 76:801–827

Preuss TM (2019) Critique of pure marmoset. Brain Behav Evol 93:92–107

Raghanti MA, Stimpson CD, Marcinkiewicz JL, Erwin JM, Hof PR, Sherwood CC (2008) Cortical dopaminergic innervation among humans, chimpanzees, and macaque monkeys: a comparative study. Neuroscience 155:203–220

Raghanti MA et al (2009) Species-specific distributions of tyrosine hydroxylase-immunoreactive neurons within the prefrontal cortex of anthropoid primates. Neuroscience 158:1551–1559

Raghanti MA et al (2016) Human-specific increase in dopaminergic innervation in a striatal region associated with speech and language: a comparative analysis of the primate basal ganglia. J Comp Neurol 524:2117–2129

Raghanti MA et al (2018) A neurochemical hypothesis for the origin of hominids. Proc Natl Acad Sci

1719666115:E1719661108–E1719661116. https://doi.org/10.1073/pnas.1719666115
Raleigh MJ, McGuire MT, Brammer GL, Pollack DB, Yuwiler A (1991) Serotonergic mechanisms promote dominance acquisition in adult male vervet monkeys. Brain Res 559:181–190
Rilling JK, Sanfey AG (2011) The neuroscience of social decision making. Annu Rev Psychol 62:23–48
Sherwood CC et al (2006) Evolution of increased glia-neuron ratios in the human frontal cortex. Proc Natl Acad Sci USA 103:13606–13611
Smaers JB, Rohlf FJ (2016) Testing species' deviation from allometric predictions using the phylogenetic regression. Evolution 70:1145–1149
Sousa AMM et al (2017) Molecular and cellular reorganization of neural circuits in the human lineage. Science 358:1027–1032
Stallen M, Sanfey AG (2015) The neuroscience of social conformity: implications for fundamental and applied research. Front Neurosci 9:337
Tachibana Y, Hikosaka O (2012) The primate central pallidum encodes expected reward value and regulates motor action. Neuron 76:826–837
Tanaka SC, Doya K, Okada G, Ueda K, Okamoto Y, Yamawaki S (2004) Prediction of immediate and future rewards differentially recruits cortico-basal ganglia loops. Nature Neurosci 7:887–893
Tanaka SC, Schweighofer N, Asahi S, Shishida K, Okamoto Y, Yamawaki S, Doya K (2007) Serotonin differentially regulates short- and long-term prediction of rewards in the ventral and dorsal striatum. PLoS ONE. https://doi.org/10.1371/journal.pone.0001333
van den Bos R (2015) The dorsal and ventral striatum play different roles in the programming of social behaviour: a tribute to Lex Cools. Behav Pharmacol 26:6–17
van den Bercken J, Cools AR (1982) Evidence for the role of the caudate nucleus in the sequential organization of behavior. Behav Brain Res 4:319–337
Volkow ND, Morales M (2015) The brain on drugs: from reward to addiction. Cell 162:712–725
Young LJ, Wang Z (2004) The neurobiology of pair bonding. Nat Neurosci 7:1048–1054
Young LJ, Wang Z, Insel TR (1998) Neuroendocrine bases of monogamy. Trends Neurosci 2:71–75
Zaki J, Schirmer J, Mitchell JP (2011) Social influence modulates the neural computation of value. Psychol Sci 22:894–900